crystals

MDPI

Review

Strategies for Optimizing the Morphology of $CsSnI_3$ Perovskite Solar Cells

Minhao Zhang [1,†], Kunli Chen [1,†], Yunxiao Wei [1], Wenzheng Hu [1], Ziyu Cai [1], Junchi Zhu [1], Qiufeng Ye [1,2,*], Feng Ye [3,*], Zebo Fang [1,2,*], Lifeng Yang [1,2,4,*] and Qifeng Liang [1,2]

1 Department of Physics and Zhejiang Engineering Research Center of MEMS, Shaoxing University, Shaoxing 312000, China
2 ShaoXin Chip Lab, Shaoxing 312000, China
3 Shangyu College, Shaoxing University, Shaoxing 312300, China
4 Shanghai Synchrotron Radiation Facility, Shanghai Advanced Research Institute, Chinese Academy of Sciences, Shanghai 201204, China
* Correspondence: 2021000026@usx.edu.cn (Q.Y.); yefeng@usx.edu.cn (F.Y.); csfzb@usx.edu.cn (Z.F.); yanglifeng@sinap.ac.cn (L.Y.)
† These authors contributed equally to this work.

Abstract: Over the past decade, organic–inorganic hybrid perovskite solar cells (PVSCs) have shown unprecedented growth in power conversion efficiency (PCE) from 3.8% to 25.7%. However, intrinsic thermal instability and lead toxicity are obstacles limiting its large–scale commercialization. Thus, all-inorganic $CsSnI_3$ perovskite has drawn remarkable interest owing to its nontoxicity, excellent thermal stability, low-cost fabrication, and spectacular photoelectric characteristics, including ideal bandgap range, long carrier lifetime, and large absorption coefficient. Many studies have shown that the device performances are closely related to the morphology and crystallinity of perovskite films. In this review, the physical properties of $CsSnI_3$ perovskite are summarized. Furthermore, this review primarily narrates the recent progress in optimizing the morphology by various strategies such as additive engineering, composition regulation, and deposition techniques, emphasizing their effects on grain sizes, film uniformity, grain boundary, and defect passivation.

Keywords: $CsSnI_3$ perovskite; photoelectric characteristic; morphology; additive engineering; composition regulation; deposition techniques

check for updates

Citation: Zhang, M.; Chen, K.; Wei, Y.; Hu, W.; Cai, Z.; Zhu, J.; Ye, Q.; Ye, F.; Fang, Z.; Yang, L.; et al. Strategies for Optimizing the Morphology of $CsSnI_3$ Perovskite Solar Cells. *Crystals* **2023**, *13*, 410. https://doi.org/10.3390/cryst13030410

Academic Editor: Ray-Hua Horng

Received: 30 January 2023
Revised: 19 February 2023
Accepted: 21 February 2023
Published: 27 February 2023

Copyright: © 2023 by the authors. Licensee MDPI, Basel, Switzerland. This article is an open access article distributed under the terms and conditions of the Creative Commons Attribution (CC BY) license (https://creativecommons.org/licenses/by/4.0/).

1. Introduction

Perovskite solar cells (PVSCs) have surged in popularity over the past decade, rapidly increasing their power conversion efficiency (PCE) from 3.8% to 25.7% [1–8]. However, the most influential organic–inorganic hybrid PVSCs are still in the immature stage of commercialization mainly due to the thermal instability of the organic composition and the toxicity of lead, which need to be treated well urgently [9–12]. The replacement of organic elements with stable inorganic components and replacing lead with nontoxic elements without sacrificing excellent photoelectric properties can be better adapted to applications [13–15]. Therefore, considerable environmentally benign lead-free perovskite materials have been developed. Among them, the full-inorganic $CsSnI_3$ perovskite can simultaneously achieve the advantages of nontoxicity as well as excellent thermal stability with a high decomposition temperature (~450 °C) [16,17].

In recent years, $CsSnI_3$ perovskite has been proven to be one of the most competitive lead–free perovskite materials for PVSCs [18–20]. In addition to the characteristics of thermal stability and low toxicity, $CsSnI_3$ has a band gap (Eg) of 1.3 eV, different from the Eg of lead-based perovskite (from 1.5 to 2.3 eV) and closer to the ideal photovoltaic Eg of 1.34 eV, which is more conducive to achieve the excellent device performance to reach the theoretical efficiency limit; the potential of $CsSnI_3$ exceeds that of hybrid perovskite [21,22].

Meanwhile, the low–cost fabrication of $CsSnI_3$ possesses spectacular photoelectric characteristics, including high absorption coefficient, low exciton binding energy, and long carrier diffusion length [23–25]. Therefore, efficient performance can be realized within the $CsSnI_3$ PVSCs.

Currently, $CsSnI_3$ PVSCs have achieved significant progress. In 2012, $CsSnI_3$ perovskite solar cells with a PCE of 0.9% were firstly fabricated by Chen et al. with an ITO/$CsSnI_3$/Au/Ti device structure [26]. In 2016, Marshall et al. codeposited perovskite precursors with $SnCl_2$, which can remove the electron barrier and suppress the pinhole density in the perovskite layer, achieving a stronger stability than $MAPbI_3$ and a PCE of 3.56% [27]. Since then, $CsSnI_3$ perovskite did not make outstanding achievements. In 2021, Yin et al. used the surface passivation strategy to achieve a photovoltaic device with 8.2% PCE [28]. Additionally, most recently, the efficiency of $CsSnI_3$, further improved by Ye et al., exceeded 10%, showing a bright promise [29]. In pursuing the development of $CsSnI_3$ PVSCs, besides solving the issues of oxidation of Sn^{2+} to Sn^{4+}, interfacial engineering, composition optimization, and morphology improvement have been studied as the main focus.

More importantly, the improvement of morphology and crystallinity of the perovskite layers are the pivotal factors to reduce defect density, leakage current, and contact resistance, aiming to prepare efficient and stable solar cells [30–34]. The purpose of morphology control is to obtain films with better uniformity, compactness, pinhole freeness, large crystal size, and excellent crystallinity. In this review, the physical properties of $CsSnI_3$ perovskite are systematically analyzed, and moreover, the present review focuses on the recent progress in optimizing the morphology by various strategies such as additive engineering, compositional regulation, and deposition methods focusing on grain sizes, film uniformity, grain boundary, and defect passivation, as illustrated in Figure 1.

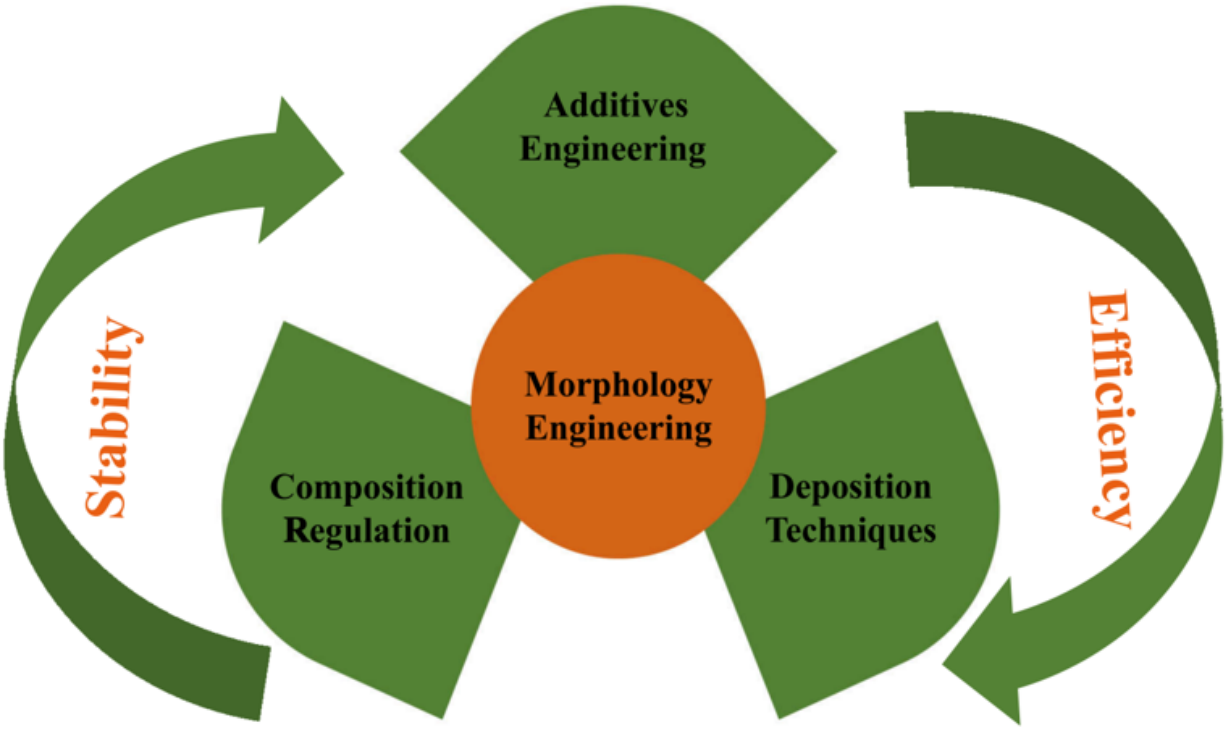


Figure 1. Classification of morphology engineering technologies for $CsSnI_3$ PVSCs.

2. Crystal Structure and Phase Transition of the $CsSnI_3$ Perovskite

2.1. Crystal Structure

Goldschmidt toleration factors can predict the structural stability of an ABX_3 perovskite depending on the degree of distortion of the BX_6 octahedron [35,36]. According to well–known theoretical calculations, perovskites are stable at t values of 0.8–1.1, whereas cubic perovskites form at t values of 0.9–1.0 [37]. Compared to $CsPbI_3$ perovskite, the $CsSnI_3$ has a t value closer to 1 because Sn^{2+} (0.112 nm) has a smaller ionic radius than Pb^{2+} (0.119 nm) [38]. Thus, all-inorganic $CsSnI_3$ perovskite is more robust and environmentally stable than lead–based perovskites (e.g., $CsPbI_3$). However, the structural stability of the $CsSnI_3$ perovskite remains a major challenge owing to the small ionic radius of Cs^+, resulting in rotation and tilt of the $[SnI_6]^{4-}$ octahedral [39,40].

2.2. Phase Transition

Similar to other phase–change materials, such as $CsPbI_3$, $CsSnI_3$ exhibits four polymorphs [41,42]. There are two types of polymorph: one is yellow in color (Y) with a one-dimensional double-strand structure, and the other is black in color (B) with a three-dimensional structure [43]. As shown in Figure 2a, at a high temperature of above 425K, $CsSnI_3$ perovskites display a phase change from the yellow Y phase to a black cubic B-α phase; with the subsequent cooling, it undergoes a degeneration in symmetry and will transform to a black tetragonal B–β phase at 380 K and a black orthorhombic B–γ phase at around 300K. When perovskite is exposed to air, the black phase (B–α, B–β, B–γ) will transform to the yellow phase (Y–phase), owing to the degree of oxidation of Sn. The local coordination environment of Cs atoms in different $CsSnI_3$ phases was also studied by Chungs et al. [43], as shown in Figure 2b–e, which can reveal the key driver behind these phase transitions. They found that the Cs atoms are randomly distributed in the perovskite lattices and the Sn–I–Sn bond is flexible enough to distort the lattice as well as to shorten the distance between the Cs and I atoms. For the cooling process of $CsSnI_3$ perovskite, the Cs atom is in the force-balanced position in the cuboctahedral geometry at 500K. At 380K, the Cs atom will have an elliptical vibration, making it have the distorted cuboctahedral geometry; thus, the distance between Cs and I will be closer. At room temperature, the Cs and I atoms will split, and the Cs atoms will deviate to one side to strongly interact with I atoms. After perovskite exposed to air and transformed to the Y phase, the Cs atoms were no longer in the lattice cage but eventually settled into a nine–coordinated tricapped trigonal prism geometry. Therefore, the local coordination environment of Cs atoms provides valuable information for the phase transition of $CsSnI_3$ perovskite.

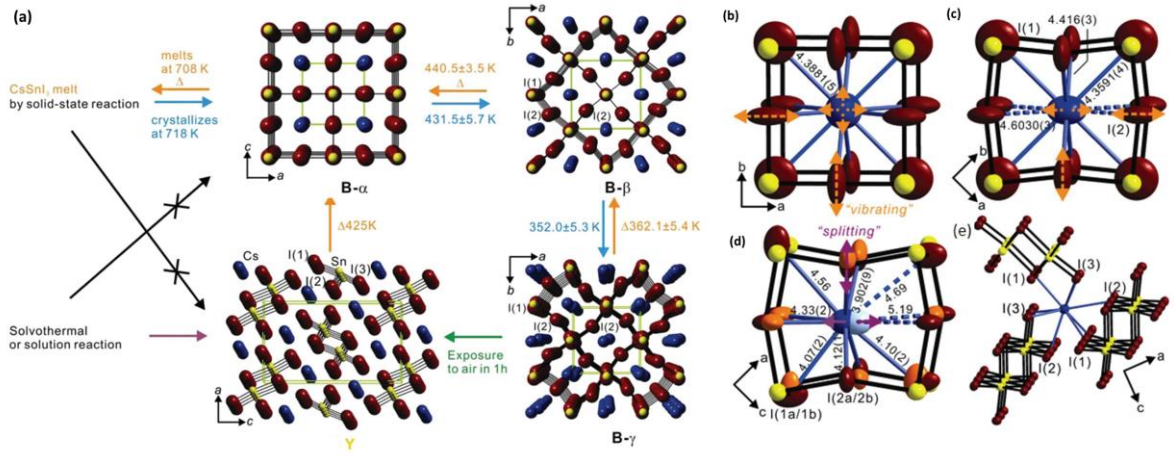


Figure 2. (**a**) Phase transition diagrams of four $CsSnI_3$ polycrystalline types; coordination environment of Cs atoms at different temperatures in the black phase (**b**) 500K (B–α), (**c**) 380K (B–β), and (**d**) 300K (B–γ); (**e**) coordination environment of Cs atoms in the yellow phase (Y) [43].

3. Morphology Control

The surface morphology of the $CsSnI_3$ perovskite has become a significant issue. High–quality film morphology plays an important role in obtaining efficient and stable $CsSnI_3$ PVSCs simultaneously. For $CsSnI_3$ PVSCs, a high–quality film morphology is effective in reducing defects and carrier traps as well as in preventing the oxidation of Sn^{2+} by oxygen and water through the pinholes. Device parameters that have a great influence on the performance of $CsSnI_3$ PVSCs, such as carrier separation ability, diffusion coefficient, and diffusion length, are also mainly determined by the crystallinity quality of perovskite films [44–47]. Through the component regulation, the introduction of various additives, and the improvement of fabrication procedures, systematic progress has been made on the perovskite morphology. Optimization of the morphology is determined by in-depth study of the characterization of the perovskite film and the photoelectric characteristics of the device, with the aim of ultimately improving the performance of PVSCs [48–50]. Generally speaking, the crystallinity of the final film depends on plentiful factors such as additive type, chemical composition, deposition techniques, and hydrophobicity. Through the morphology control strategy, the crystallinity in perovskite films can be effectively optimized. Specifically, uniform grains and high surface coverage can be achieved, which is conducive to carrier transport.

3.1. Additive Engineering

In 2012, Chen et al. first applied inorganic $CsSnI_3$ perovskite without any additives as the light-sensitive layer to fabricate a Schottky device [26]. The relatively poor device performance, with PCE less than 1% and a large ideality factor n of 2.8, which is related to the charge recombination, proved the inferior film quality and surface state [51–53]. Doping various additives in the $CsSnI_3$ perovskite film, such as inorganic halide salts such as SnX_2 (X=F, Cl, Br, I) and organic reducing additives such as some polymers and organic salts, is one of the effective ways to improve its film quality and surface morphology. Different additives have their own unique effects on morphology; generally speaking, additives can improve film crystallinity, reduce defects, improve carrier transport capacity, and ultimately affect the device performance [54,55].

3.1.1. SnX_2 (X=F, Cl, Br, I)

The introduction of SnX_2 additives can mainly precipitate more crystal growth nuclei, form a thin nanolayer at the grain boundaries, and modify the surface state, contributing to make the film more uniform and of higher coverage. This modification can result in the optimization of the film morphology and therefore can be considered as an effective strategy to improve the quality of the $CsSnI_3$ perovskite.

SnI_2: Marshall et al. reported a promising method to simultaneously improve the efficiency and stability of $CsSnI_3$ devices by using excessive SnI_2 during the synthesis of $CsSnI_3$. The optimized $CsSnI_3$ perovskite films showed a larger mean crystallite size, fewer pin holes, and more reduced background carrier density. As a result, at the optimal content of excessive SnI_2, the PVSCs achieved a PCE of 2.76% and a high V_{oc} of 0.55 V [56]. Inspired by the work of Marshall et al., the effect of excessive SnI_2 on the performance of the $CsSnI_3$ perovskite device was also explored by Song et al. [57]. They argued that SnI_2 does not disturb the formation of $CsSnI_3$ film, but disperses uniformly within the films or forms a very thin nanolayer at the grain boundaries of $CsSnI_3$ to promote a film with better coverage and fewer pinholes, as shown in Figure 3a. At the optimal CsI/SnI_2 ratio of 0.4, the modified $CsSnI_3$ PVSC under hydrazine atmosphere realized a PCE of 4.81%.

$SnBr_2$: In 2018, Heo et al. compared the impact of SnX_2 additives (X=F, Cl, Br) in $CsSnI_3$ PVSCs. As shown in Figure 3b, when the $SnBr_2$ additive is added, the surface adsorption energy of $CsSnI_3$ perovskite is minimal, and the surface formation energy of perovskite is also reduced, greatly suppressing the defects in the film. Furthermore, as shown in Figure 3c–f, the addition of $SnBr_2$ can inhibit phase separation and thus further

improve the film morphology. As a result, devices with the $SnBr_2$ additive are more stable and efficient, showing 100 h of storage stability as well as a PCE of 4.3 % [58].

$SnCl_2$: Marshall et al. also studied the impact of the SnX_2 (X = F, Cl, Br, I) additives on the morphology of the $CsSnI_3$ films and the performance of the $CsSnI_3$ PVSCs. Figure 3g shows the scanning electron microscope (SEM) of the films with the different SnX_2 additives (X=F, Cl, Br, I); all additives showed significant improvements in the quality of the perovskite films. Among the SnX_2 (F, Cl, Br, I) additives, the authors argued that $SnCl_2$ could form a thin film on the surface of the perovskite, and therefore modified the surface state. It acted as a desiccant and sacrificial layer to absorb water, as schematically illustrated in Figure 3g. Finally, by adding $SnCl_2$, the perovskite device delivered a PCE of 3.56% and excellent stability, as shown in Figure 3h–i [27].

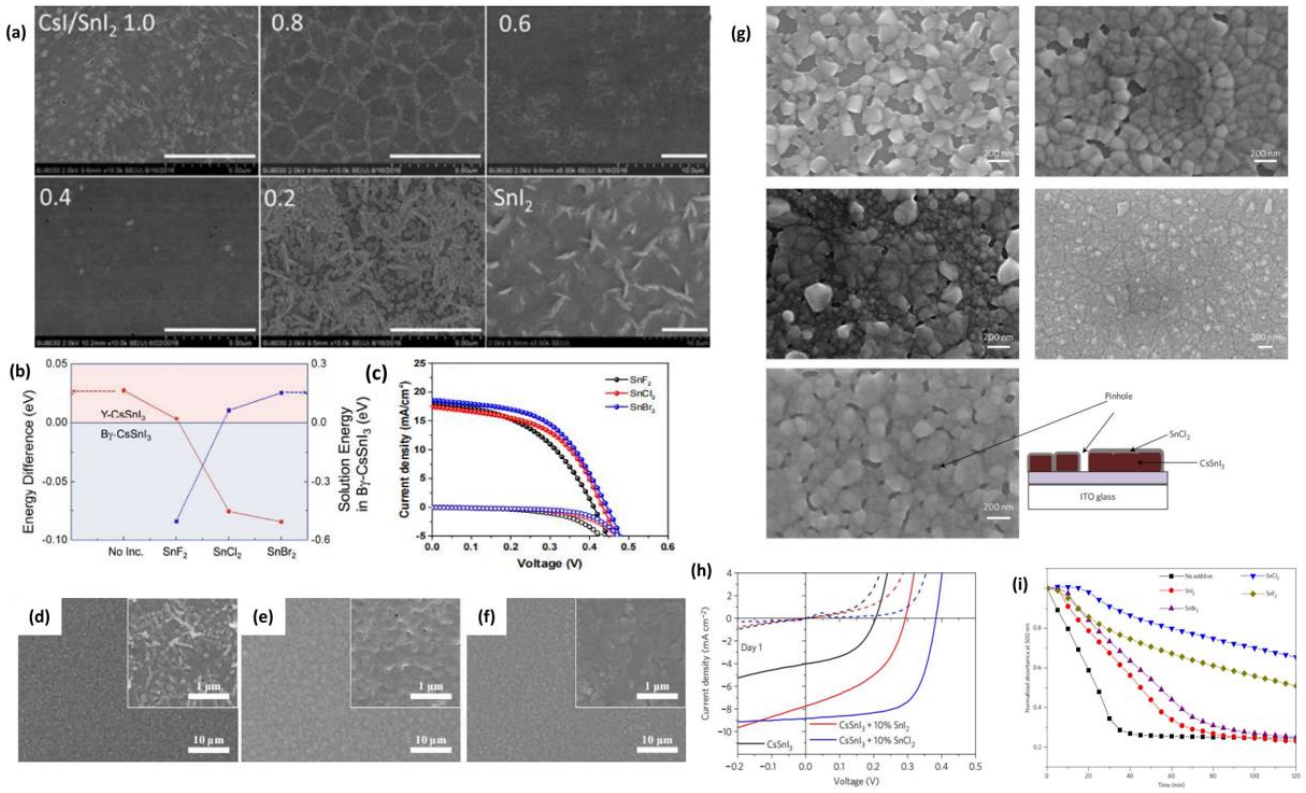


Figure 3. (**a**) SEM pictures of $CsSnI_3$ perovskite films with different molar ratios of CsI/SnI_2 [57]. (**b**) Total energy discrepancy between different phases of $CsSnI_3$. (**c**) Performances of $CsSnI_3$ PVSCs with different additives. The SEM surface pictures of $CsSnI_3$ perovskite films with different additives (**d**) SnF_2, (**e**) $SnCl_2$, and (**f**) $SnBr_2$ additives [58]. (**g**) SEM images of $CsSnI_3$ films prepared under different conditions containing no tin halide additive, 10 mol% SnI_2, 10 mol% $SnBr_2$, 10 mol% SnF_2, and 10 mol% $SnCl_2$. (**h**) J–V performance and (**i**) stability of $CsSnI_3$ PVSCs prepared under different conditions containing without additive, 10 mol% SnI_2, 10 mol% $SnBr_2$, 10 mol% SnF_2, and 10 mol% $SnCl_2$ [27].

SnF_2: SnF_2 is commonly applied to improve the morphology and coverage of Sn–based perovskite as well as play the role of antioxidant [59]. Liao et al. found that the flower-shaped structure of the initial film without additives disappears with the increase in SnF_2 in $FASnI_3$ perovskite. Meanwhile, SnF_2 also inhibits the oxidation of Sn^{2+}, maintaining a reduction environment. Inspired by this idea, Kumar et al. added SnF_2 into $CsSnI_3$ and improved the quality of perovskite. The background carrier density and tin vacancy were reduced. Finally, the modified solar cells with the structure of FTO/compact TiO_2/mesoporous TiO_2/$CsSnI_3$/HTM/Au were achieved with a top PCE of 2.02% [60].

What's more, it has been found that adding the SnF_2 additive to $CsSnI_3$ is helpful to improve light stability and optimize band alignment at the perovskite interfaces.

3.1.2. Reductive Organic Additives

As mentioned above, the introduction of the SnX_2 additive can improve the morphology quality of perovskite films, which is extremely important for the performance of $CsSnI_3$ PVSCs. However, in terms of this single strategy, the improvement in PVSCs' performance is not significant enough (PCE < 5%), mainly due to the fact that Sn^{2+} tends to oxidize to Sn^{4+} even in the presence of SnX_2 during and after $CsSnI_3$ film formation [61]. Meanwhile, SnX_2 will also cause phase separation of halide perovskite [62]. Fortunately, it was found that reductive organic additives can further provide a strong reduction environment for Sn^{2+}, effectively inhibiting the oxidation of Sn^{2+} and the generation of Sn vacancy. More significantly, organic additives can improve the morphology of perovskite films and promote the performance of devices.

Wang et al. used a coadditive 2–aminopyrazine (APZ) as a secondary addition to the $CsSnI_3$–20% SnF_2 perovskite solution to form the APZ–SnF_2 complex, with the aim of inhibiting the oxidation of Sn^{2+}, achieving uniform films, and finally improving the $CsSnI_3$-based device performance. Figure 4a illustrates the process for the preparation and morphology of $CsSnI_3$ films with different additives (SnF_2 alone and the SnF_2–APZ complex). This strategy can efficiently enable the homogeneous spread of SnF_2 in perovskite films and promote the ordered crystallization and growth of the perovskite layer. The introduction of APZ also greatly inhibits the oxidation of Sn^{2+} in $CsSnI_3$ perovskite owing to the electron-donating effect contributed by the amino group in APZ (Figure 4b). More importantly, as shown in Figure 4c, compared to the initial perovskite morphology with cobblestone-like aggregations and many pinholes on the surface, the resulting film with the APZ–SnF_2 complex showed a denser and smoother surface. Consequently, optimized $CsSnI_3$ PVSCs that used a printable c–TiO_2/m–TiO_2/Al_2O_3/NiOx/carbon structure achieved a PCE of 5.12% [63]. The reductive additive cobaltocene (denoted $CoCp_2$) was also utilized by Wang et al. to modify the $CsSnI_3$ perovskite, as illustrated in Figure 4d, which achieved enhanced performance, suppressed Sn^{2+} oxidation, and improved film morphology, as shown in Figure 4e [64].

Due to the advantages of reductive organic additives, organic compounds of reductive properties and containing multiple electron–donating groups are applied to $CsSnI_3$ perovskite to inhibit the Sn^{2+} oxidation to decrease defect density and improve film morphology. Ye et al. introduced N,N'–methylenebis(acrylamide) (MBAA) with the –NH and –CO groups into the B–γ $CsSnI_3$ perovskite layer. The lone electron pairs on the –NH and –CO groups can form a coordination bond with Sn^{2+}, thus causing a reduced defect (Sn^{4+}) density and a smoother and denser morphology, as shown in Figure 4f. Correspondingly, a high PCE of 7.5% was achieved with excellent device stability [65]. Phthalimide (PTM) that has the same chemical groups of –NH and –CO was also utilized by the Ye group into the B–γ $CsSnI_3$ perovskite layer, as illustrated in Figure 4g. PTM could uniformly cover the $CsSnI_3$ perovskite particles. Meanwhile, the strong coordination effect between PTM and perovskite makes it act as an adhesive to bind adjacent perovskite grains and form a compact and smooth crystal perovskite film. Optimized PTM–$CsSnI_3$ PVSCs with a device structure of ITO/PEDOT:PSS/PTM–$CsSnI_3$/indene-C60 bis–adduct (ICBA)/BCP/Ag showed a record PCE of 10.1% with excellent thermal and light stability [29].

In addition to the organic compounds mentioned above, other reductive organic additives such as piperazine (Figure 4h), ascorbic acid, thiosemicarbazide (TSC), and hydrazine [28,66–68] with Lewis base groups have also been widely used to improve the quality of perovskite films. Therefore, these encouraging results provide a promising strategy for the preparation of environmentally friendly high–performance $CsSnI_3$ PVSCs.

3.2. Composition Regulation

Unlike additive engineering, component regulation is the optimization of the component elements in each position of the perovskite. It is well–known that lead-based ABX_3 perovskite can be partially substituted by other ions to modify the photoelectric performance by enhancing the quality of the perovskite film and the stability of solar cells [69–74]. Therefore, these strategies are also used in $CsSnI_3$ perovskite to adjust tolerance factors, optimize film morphology, and reduce defect density.

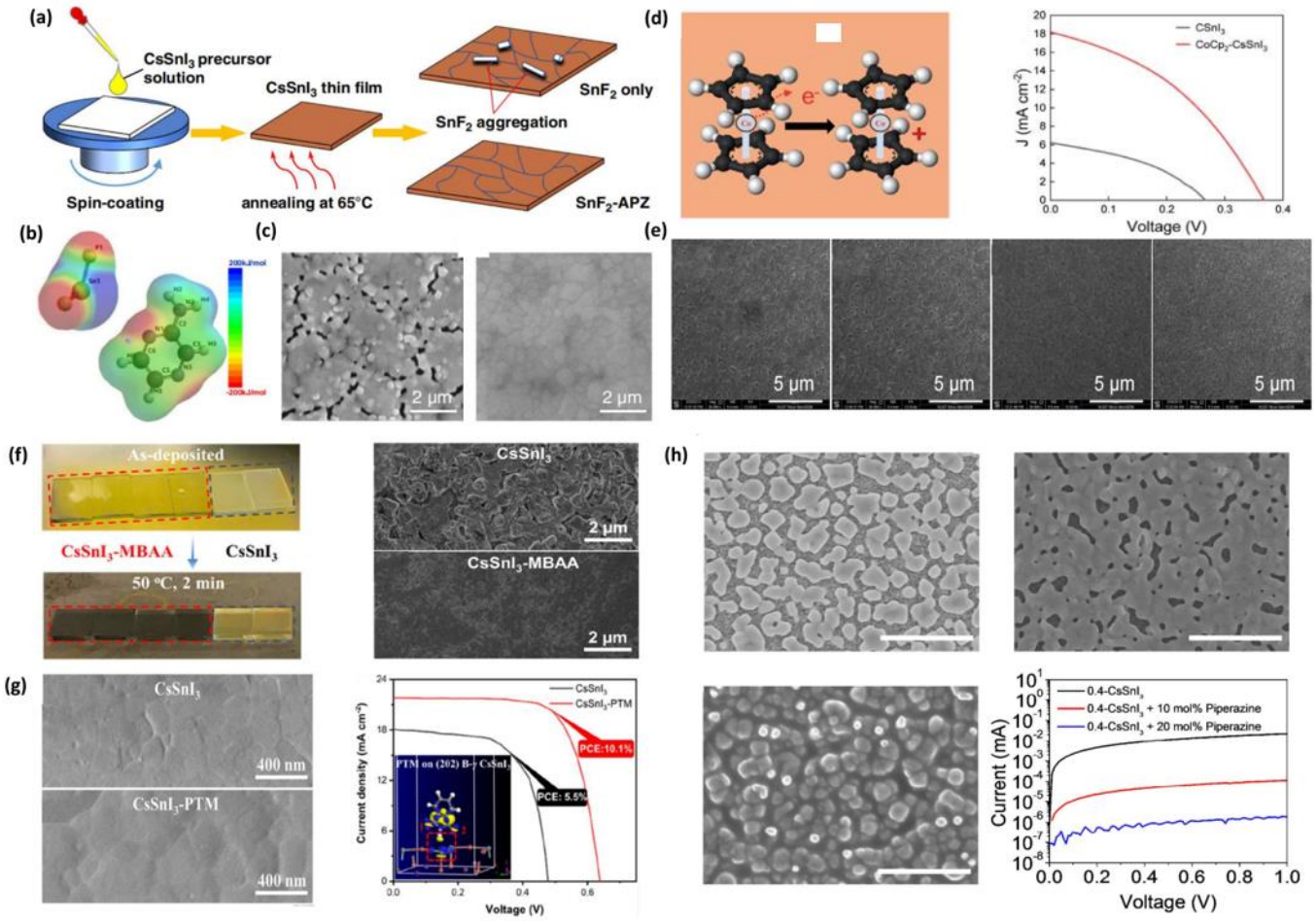


Figure 4. (**a**) Illustration for the preparation of $CsSnI_3$ films with SnF_2 and SnF_2–APZ complex. (**b**) Electrostatic potential surfaces for SnF_2 and APZ. (**c**) Top–view SEM pictures of $CsSnI_3$ films with 0% APZ and 10 mol% APZ additives [63]. (**d**) Schematic illustration of $CoCp_2$'s redox property and J–V curves of $CsSnI_3$ PVSCs with and without $CoCp_2$. (**e**) Top–view SEM images of $CsSnI_3$ films without and with different content of $CoCp_2$: 0%, 0.5%, 1%, and 2% [64]. (**f**) The images show the color changes of the $CsSnI_3$ films with and without MBAA [29]. (**g**) Surface SEM images and performance of the $CsSnI_3$ and $CsSnI_3$–PTM samples, respectively [66]. (**h**) SEM images and I–V characteristics of 0.4–$CsSnI_3$ perovskite films prepared with different concentrations of piperazine; scale bars are 2 μm [65].

A site: Marshall et al. systematically studied the effect of Rb^+ partial replacement of Cs^+ on the $CsSnI_3$ perovskite. The Cs^+ ion is located in the center of the ABX_3 perovskite cage. If it is replaced by Rb^+ of a smaller ionic radius, the crystal will tighten and the lattice will be distorted, which indirectly affects the band gap of the perovskite and the stability of perovskite. With a finite range of Rb^+ density, it is found that perovskite is stable enough to be used as the absorption layer when the density of Rb^+ is less than 0.2, and when Rb^+ exceeds 50%, $Cs_{1-x}Rb_xSnI_3$ will not form a three–dimensional perovskite structure. As

a result, the optimized PVSC based on the $Cs_{1-x}Rb_xSnI_3$ film showed an increase in Voc, demonstrating that the doping of Rb into B–γ $CsSnI_3$ perovskite is an effective strategy to increase device performance without obviously sacrificing light absorption [75].

B site: Cations at the B site occupy the lattice corner of the ABX_3 perovskite and have a significant effect on the electronic structure of the conduction and valence bands. Therefore, partial ion substitution at the B site can also optimize the properties and film quality of perovskite. Germanium (Ge) is in the same group of Sn and has a similar elemental property. Therefore, Ge could be used to replace Sn to improve the performance and stability of $CsSnI_3$ perovskite [76]. Most recently, Chen et al. introduced Ge into $CsSnI_3$ and used the solid solution perovskite as the light absorber. As shown in Figure 5a–b, they found that due to the extremely high oxidation activity of Ge, an ultrathin and uniform primary oxide surface passivating layer formed on the surface of the perovskite, which could inhibit the recombination of interface carriers and enhance the thermodynamic stability of the perovskite. Meanwhile, the perovskite layers prepared by the melt–crystallization method have ultrasmooth surfaces, as illustrated in Figure 5c. Finally, fabricated perovskite solar cells showed a PCE of 7.11%. More importantly, PVSCs also showed excellent stability, maintaining above 90% PCE after 500 h of continuous operation in N_2 atmosphere under one-sun illumination [77].

In addition to Ge, doping with other metal elements, such as Sb and Bi doping, are also an effective means to improve the crystallinity and performance of lead-based perovskite solar cells [78–80]. Inspired by this, Lee et al. studied the effects of Sb and Bi doping on $CsSnI_3$ perovskite. They found that MI_3 (M=Sb, Bi) doping can improve crystallinity and reduce the formation energy of B–γ phase $CsSnI_3$, thus ensuring that the stability of the perovskite can be greatly improved. As a result, the MI_3–doped $CsSnI_3$ PVSCs became thermodynamically more stable. B–γ $CsSnI_3$ perovskites doped with 3 mol% SbI_3 and BiI_3 maintained 96% and 77% of their crystal structure, respectively, after exposure to air with a relative humidity of 45–55% for 12 h [81].

X site: X are mainly halide anions located in the vertices of the $[BX_6]^{4+}$ octahedral, which have an impact not only on the crystal structure of perovskite materials but also on their film quality and photoelectric properties [82–85]. Therefore, halide anions doping is an effective strategy for regulating the quality of perovskite films and device performance. Sabba et al. modulated the open–circuit voltage and photoelectric properties of $CsSnI_3$ by chemically doping Br to form the $CsSnI_{3-x}Br_x$ ($0 \leq x \leq 3$) perovskite. As can be seen in Figure 5d–g, when perovskite is in the form of $CsSnI_2Br$, the original film of $CsSnI_3$ perovskite with multiple pinholes becomes dense and smooth. A further increase in Br doping amount will lead to some island-shaped grains forming on the surface of the perovskite until it becomes rough for $CsSnBr_3$. Therefore, there exists an optimal Br doping, at which the morphology of thin films is significantly improved. Figure 5h shows that the bandgap of $CsSnI_{3-x}Br_x$ increased gradually with increasing Br content, which will reduce light absorption but will be beneficial for enhancing Voc. As a result, a Voc enhancement was achieved in $CsSnI_{3-x}Br_x$ PVSCs, as the I ions were gradually substituted by Br [86]. Zhao et al. modified the crystal structure of B–γ $CsSnI_3$ perovskite by chemically doping Br to form the $CsSnI_{3-x}F_x$ ($0 \leq x \leq 3$) perovskite. Figure 5i shows the macroscopic images of the color evolution in the $CsSnI_{3-x}F_x$ films, and it can be observed that the appearance of the perovskite film becomes visually lighter as the I ions are gradually substituted by F. It is found that the evolution of color slows down as the F ratio in the films increases, which indicates that the stability is enhanced [87].

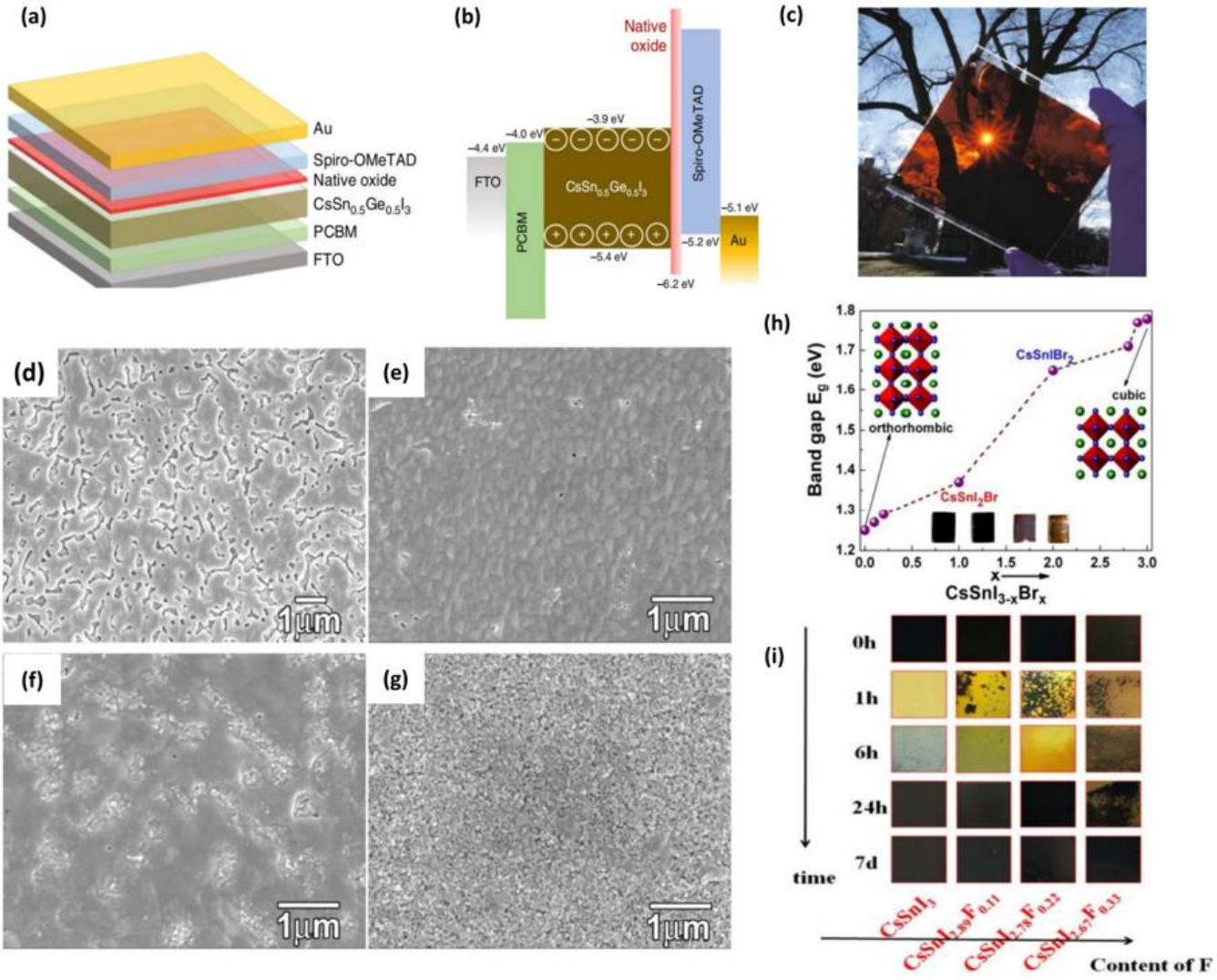


Figure 5. (**a**) Schematic illustration of the device structure of the $CsSn_{0.5}Ge_{0.5}I_3$ PVSC. (**b**) Corresponding device energy-level diagram. (**c**) Schematic illustration showing the deposition of ultrasmooth $CsSn_{0.5}Ge_{0.5}I_3$ perovskite film [77]. (**d**–**g**) Top–view SEM images of $CsSnI_3$, $CsSnI_2Br$, $CsSnIBr_2$, and $CsSnBr_3$ displaying the morphological evolution. (**h**) The band gap variation with Br concentration [86]. (**i**) Macroscopic images of the color evolution in $CsSnI_{3-x}F_x$ films [87].

3.3. Deposition Techniques

Homogeneous and dense perovskite thin films are essential for the preparation of highly efficient and stable $CsSnI_3$ PVSCs, and the quality of perovskite thin films is closely related to the deposition techniques. Therefore, the development of advanced and highly reproducible deposition techniques is the key to the preparation of high–performance devices. Currently, the commonly used deposition methods for $CsSnI_3$ PVSCs include the conventional solution technique, evaporation–assisted solution (EAS) technique [88], vacuum flash–assisted solution processing (VASP) technique [89], and pulsed–laser deposition (PLD) technique [90].

Solution techniques fall into two categories: the one–step solution technique and the two–step solution technique [91,92]. Because the latter has a poorer effect on $CsSnI_3$ perovskite, it is rarely used. The one–step solution technique has become the most frequently used deposition technique for the preparation of $CsSnI_3$ perovskite films because of its simple preparation technique, high film–forming reproducibility, and environmental friendliness. The quality of $CsSnI_3$ perovskite films can be improved during spin coating with

the help of antisolvent [93]. However, the fabrication of high–quality $CsSnI_3$ perovskite films using the conventional solution technique remains a challenge. Thus, it is significant for the development of new deposition techniques.

In 2016, a new technique of thermally driven solid-state coarsening was applied by Wang et al. to achieve high-quality B–γ $CsSnI_3$ perovskite films [94]. Figure 6a shows the preparation of B–γ–$CsSnI_3$ thin films and the morphology evolution of deposited B-γ-$CsSnI_3$ thin films driven by coarse graining with an increase in the temperature of heat treatment. They dissolved solid $CsSnI_3$ perovskite in a mixture of methoxyacetonitrile, dimethyl formamide, and acetonitrile, then spin-coated on the substrate. After that, different annealing temperatures are set to the as-deposited films to facilitate crystallization. As shown in Figure 6b, with the increase in annealing temperature, the grain size of B–γ $CsSnI_3$ perovskite gradually grew, and the grain boundary decreased. As a result, at a moderate temperature of 150 °C, the $CsSnI_3$ perovskite film with large grain size and extremely smooth morphology were realized, and the optimized device with a structure of ITO/NiOx/$CsSnI_3$/PCBM/Al achieved a PCE of 3.31%. Similar annealing methods for controlling solvent growth were also been used by Ban et al. in 2022. The group proposed an effective two-step thermal annealing method to modulate the dynamic balance between the perovskite crystals' growth and nucleation for the black B–γ phase $CsSnI_3$ perovskite, as shown in Figure 6c. The well-crystallized and smooth $CsSnI_3$ thin films can be obtained after a two-step temperature annealing process with temperatures of 40 °C and 70 °C, respectively, as shown in Figure 6d. With the further introduction of 1–(4–carboxyphenyl)–2–thiourea to coordinate with surface undercoordinated Sn^{2+} cations of $CsSnI_3$ thin films, the defect density decreased significantly, and the modified device with a printable c–TiO_2/m–TiO_2/Al_2O_3/NiOx/carbon mesoporous framework achieved a PCE of 8.03%. The device showed excellent stability, as it maintained 90% of the initial efficiency after 3000 h of storage in a N_2–filled glovebox [95].

The evaporation–assisted solution (EAS) technique provides a new way to prepare high–quality perovskite films. In 2018, Zhu et al. employed the EAS technique, combining thermal evaporation with the solution technique to produce rather uniform, dense, and pinhole–free $CsSnI_3$ films. As shown in Figure 6e, the SnI_2 solution with SnF_2 was first spin coated on the mesoporous TiO_2. After annealing, the resultant film was transferred to a vacuum chamber for the next step of the CsI deposition. After precisely controlling the evaporation rate and the final thickness of the CsI was deposed onto the SnI_2–SnF_2 layer, the prefabricated film was eventually annealed at 150 °C and formed a black B–γ $CsSnI_3$ perovskite. By comparing the morphology of $CsSnI_3$ perovskite films with different CsI thicknesses, as illustrated in Figure 6f, it is obvious that the quality of the perovskite film has improved remarkably when the thicknesses of CsI are optimized. As a result, the $CsSnI_3$ PVSCs fabricated by the EAS technique delivered a best PCE of 2.23% [88].

The evaporation technique is a better method for the preparation of a large-area perovskite without the bondage of the solution. An effective passivator–assisting sequential vapor deposition (PASVD) strategy was demonstrated by Yin et al. [28], combining the synergistic advantage of vapor deposition and surface passivation, as shown in Figure 6g. The fabricated $CsSnI_3$ perovskite with low densities in the deep trap state was achieved, which was attributed to the smoother compact morphology (Figure 6h) and the low molecular weight organic passivators: thiosemicarbazide (TSC). With this strategy, the $CsSnI_3$ PVSCs with an inverted 'p–i–n' structure of ITO/PEDOT:PSS/$CsSnI_3$/C60/BCP/Cu achieved a high PCE of 8.2%, as shown in Figure 6j.

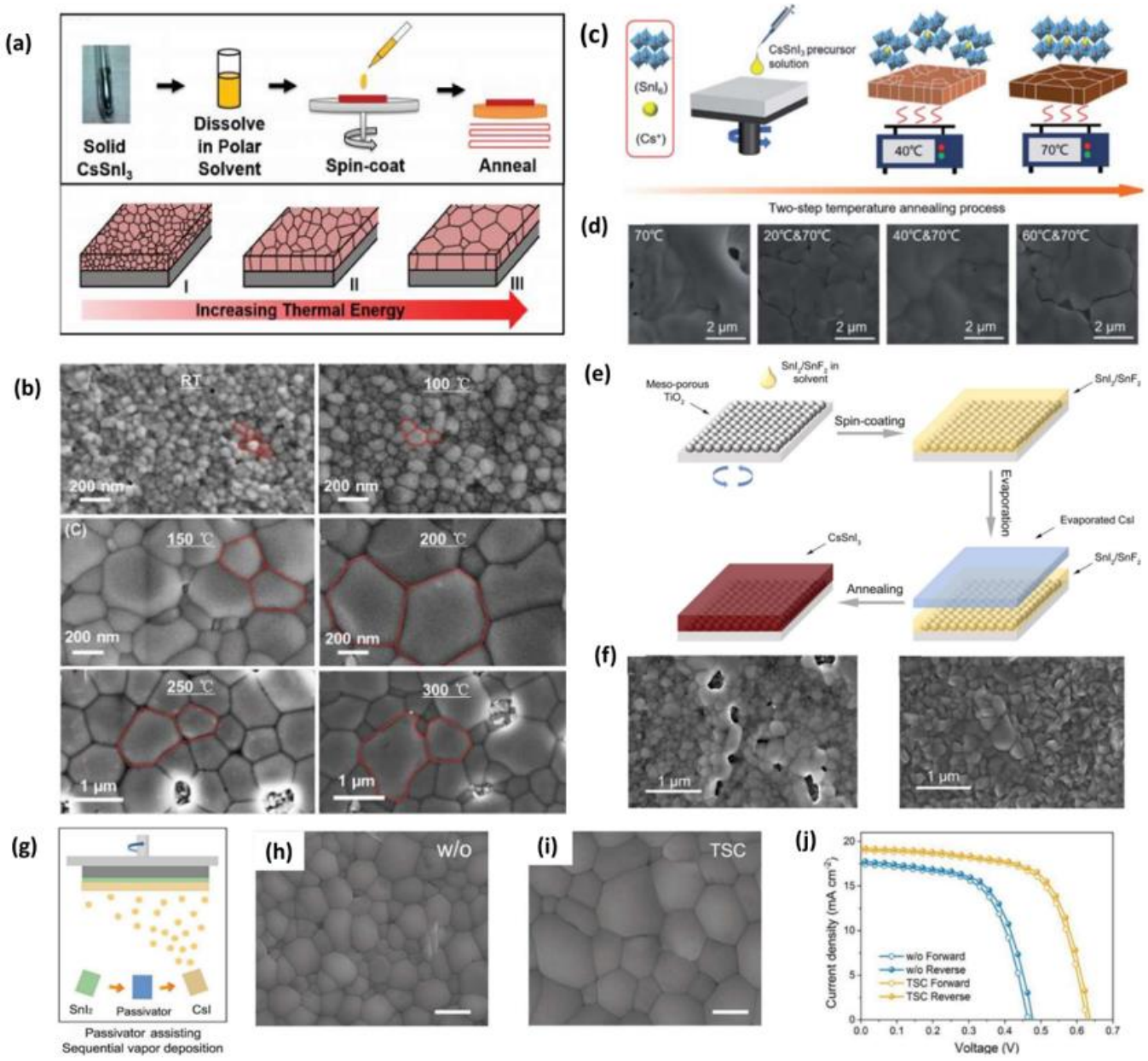


Figure 6. (**a**) Illustration of one-step solution fabrication and the grain-coarsening driven morphology evolution of as–deposited B–γ–$CsSnI_3$ thin film with increasing heat–treatment temperature. (**b**) SEM pictures of the $CsSnI_3$ films annealed at different temperatures [94]. (**c**) Illustration of the two-step temperature annealing process of B–γ–$CsSnI_3$ thin films. (**d**) Surface SEM images of $CsSnI_3$ films employing different annealing procedures [95]. (**e**) Schematic representation of the evaporation–assisted solution technique. (**f**) Top–view SEM pictures of annealed $CsSnI_3$ films with different CsI thicknesses [88]. (**g**) Schematic representation of the PASVD technique for fabricating $CsSnI_3$ perovskite films. (**h**,**i**) SEM pictures of $CsSnI_3$ films without and with TSC addition. (**j**) The best performance for with and without TSC passivated of $CsSnI_3$ PVSCs [28].

4. Conclusions and Summary

The surface morphology has become the key issue that affects the performance of $CsSnI_3$ PVSCs and is now the subject of the greatest attention. Through the morphology control strategy, the crystallinity of the perovskite film can be effectively improved. Specifically, uniform grains and high surface coverage can be achieved, which is conducive to carrier transport and finally has a positive impact on the efficiency and stability of the solar

cells. Herein, the physical properties of $CsSnI_3$ PVSCs were summarized. In addition, we focused on the recent progress in optimizing morphology using various strategies such as additive engineering, compositional regulation, and deposition techniques as shown in Table 1, especially their effects on grain sizes, film uniformity, grain boundary, and defect passivation.

Table 1. Summary of morphological engineering strategies for $CsSnI_3$ PVSCs.

Morphological Engineering Strategies	Device PCE	Ref.
Additive Engineering		
10 mol% excess SnI_2	2.76%	[56]
CsI/SnI_2 ratio of 0.4	4.81%	[57]
Perovskite film doped with $SnBr_2$	4.3%	[58]
Perovskite film doped with $SnCl_2$	3.56%	[27]
Perovskite film doped with SnF_2	2.02%	[60]
Coadditive 2–aminopyrazine (APZ)	5.12%	[63]
Cobaltocene (denoted $CoCp_2$)	3.0%	[64]
N,N′–methylenebis(acrylamide) (MBAA)	7.5%	[65]
Piperazine	3.83%	[66]
Thiosemicarbazide (TSC)	8.2%	[28]
Hydrazine	4.81%	[68]
Phthalimide (PTM)	10.1%	[29]
Composition Regulation		
$CsSn_{0.5}Ge_{0.5}I_3$	7.11%	[77]
Deposition Techniques		
Thermally driven solid–state coarsening technique	3.31%	[94]
Two–step thermal annealing process	8.03%	[95]
Evaporation–assisted solution (EAS) technique	2.23%	[88]
Passivator–assisting sequential vapor deposition (PASVD) technique	8.2%	[28]

Although there has been much research on improving the morphology of $CsSnI_3$ perovskite, the mechanism of additive engineering and component engineering is still unclear. We emphasize that the oxidation resistance and morphology control of $CsSnI_3$ are two key points for the improvement of device performance. For the practical application of $CsSnI_3$ in solar cells, there is still a lot of work to do for the stability of the B–γ $CsSnI_3$ phase. We hope to find more methods to stabilize and optimize black B–γ $CsSnI_3$ films in future studies and gain a deeper understanding of their mechanism.

Author Contributions: Writing—original draft preparation, Q.Y. and Q.L.; Writing—review and editing, M.Z., Q.Y., Z.F., F.Y., L.Y. and Q.L.; Information collection, Y.W., W.H., Z.C., K.C. and J.Z. All authors have read and agreed to the published version of the manuscript.

Funding: This work was financially supported by the Natural Science Foundation of Zhejiang Province, China (Grant Nos. LQ22F040001), China Postdoctoral Science Foundation (Grant No. 2022M723281), the Zhejiang Province Public Welfare Technology Application Research Project (Grant Nos. LGG20E030003), and the National Natural Science Foundation of China (Grant Nos. 12204313, 51872186).

Institutional Review Board Statement: Not applicable.

Informed Consent Statement: Not applicable.

Data Availability Statement: Not applicable.

Conflicts of Interest: The authors declare no conflict of interest.

References

1. Kojima, A.; Teshima, K.; Shirai, Y.; Miyasaka, T. Organometal Halide Perovskites as Visible-Light Sensitizers for Photovoltaic Cells. *J. Am. Chem. Soc.* **2009**, *131*, 6050–6051. [CrossRef] [PubMed]
2. Jiang, Q.; Zhang, L.; Wang, H.; Yang, X.; Meng, J.; Liu, H.; Yin, Z.; Wu, J.; Zhang, X.; You, J. Enhanced electron extraction using SnO_2 for high-efficiency planar-structure $HC(NH_2)_2PbI_3$-based perovskite solar cells. *Nat. Energy* **2016**, *2*, 16177. [CrossRef]
3. Park, N.-G.; Grätzel, M.; Miyasaka, T.; Zhu, K.; Emery, K. Towards stable and commercially available perovskite solar cells. *Nat. Energy* **2016**, *1*, 16152. [CrossRef]
4. Tan, H.; Jain, A.; Voznyy, O.; Lan, X.; de Arquer, F.P.G.; Fan, J.Z.; Quintero-Bermudez, R.; Yuan, M.; Zhang, B.; Zhao, Y.; et al. Efficient and stable solution-processed planar perovskite solar cells via contact passivation. *Science* **2017**, *355*, 722–726. [CrossRef]
5. Rong, Y.; Hu, Y.; Mei, A.; Tan, H.; Saidaminov, M.I.; Seok, S.I.; McGehee, M.D.; Sargent, E.H.; Han, H. Challenges for commercializing perovskite solar cells. *Science* **2018**, *361*, eaat8235. [CrossRef] [PubMed]
6. Jiang, Q.; Zhao, Y.; Zhang, X.; Yang, X.; Chen, Y.; Chu, Z.; Ye, Q.; Li, X.; Yin, Z.; You, J. Surface passivation of perovskite film for efficient solar cells. *Nat. Photonics* **2019**, *13*, 460–466. [CrossRef]
7. Luo, J.; Xia, J.; Yang, H.; Sun, C.; Li, N.; Malik, H.A.; Shu, H.; Wan, Z.; Zhang, H.; Brabec, C.J.; et al. A pressure process for efficient and stable perovskite solar cells. *Nano Energy* **2020**, *77*, 105063. [CrossRef]
8. Zhao, Y.; Ma, F.; Qu, Z.; Yu, S.; Shen, T.; Deng, H.X.; Chu, X.; Peng, X.; Yuan, Y.; Zhang, X.; et al. Inactive (PbI2)2RbCl stabilizes perovskite films for efficient solar cells. *Science* **2022**, *377*, 531–534. [CrossRef]
9. Hodes, G.; Cahen, D. Perovskite cells roll forward. *Nat. Photonics* **2014**, *8*, 87–88. [CrossRef]
10. Shi, Z.; Guo, J.; Chen, Y.; Li, Q.; Pan, Y.; Zhang, H.; Xia, Y.; Huang, W. Lead-Free Organic-Inorganic Hybrid Perovskites for Photovoltaic Applications: Recent Advances and Perspectives. *Adv. Mater.* **2017**, *29*, 1605005. [CrossRef]
11. Boix, P.P.; Agarwala, S.; Koh, T.M.; Mathews, N.; Mhaisalkar, S.G. Perovskite Solar Cells: Beyond Methylammonium Lead Iodide. *J. Phys. Chem. Lett.* **2015**, *6*, 898–907. [CrossRef] [PubMed]
12. Grätzel, M. The light and shade of perovskite solar cells. *Nat. Mater.* **2014**, *13*, 838–842. [CrossRef] [PubMed]
13. Jia, X.; Zuo, C.; Tao, S.; Sun, K.; Zhao, Y.; Yang, S.; Cheng, M.; Wang, M.; Yuan, Y.; Yang, J.; et al. $CsPb(I_xBr_{1-x})_3$ solar cells. *Sci. Bull.* **2019**, *64*, 1532–1539. [CrossRef] [PubMed]
14. Tai, Q.; Tang, K.-C.; Yan, F. Recent progress of inorganic perovskite solar cells. *Energy Environ. Sci.* **2019**, *12*, 2375–2405. [CrossRef]
15. Li, B.; Fu, L.; Li, S.; Li, H.; Pan, L.; Wang, L.; Chang, B.; Yin, L. Pathways toward high-performance inorganic perovskite solar cells: Challenges and strategies. *J. Mater. Chem. A* **2019**, *7*, 20494–20518. [CrossRef]
16. Chung, I.; Lee, B.; He, J.; Chang, R.P.H.; Kanatzidis, M.G. All-solid-state dye-sensitized solar cells with high efficiency. *Nature* **2012**, *485*, 486–489. [CrossRef] [PubMed]
17. Stoumpos, C.C.; Malliakas, C.D.; Kanatzidis, M.G. Semiconducting Tin and Lead Iodide Perovskites with Organic Cations: Phase Transitions, High Mobilities, and Near-Infrared Photoluminescent Properties. *Inorg. Chem.* **2013**, *52*, 9019–9038. [CrossRef] [PubMed]
18. Aamir, M.; Adhikari, T.; Sher, M.; Khan, M.D.; Akhtar, J.; Nunzi, J.-M. Cesium Lead Halide Perovskite Nanostructures: Tunable Morphology and Halide Composition. *Chem. Rec.* **2017**, *18*, 230–238. [CrossRef] [PubMed]
19. Patrick, C.E.; Jacobsen, K.W.; Thygesen, K.S. Anharmonic stabilization and band gap renormalization in the perovskite $CsSnI_3$. *Phys. Rev. B* **2015**, *92*, 201205. [CrossRef]
20. Kang, C.; Rao, H.; Fang, Y.; Zeng, J.; Pan, Z.; Zhong, X. Antioxidative stannous oxalate derived lead-free stable $CsSnX_3$ (X= Cl, Br, and I) perovskite nanocrystals. *Angew. Chem. Int. Ed.* **2021**, *133*, 670–675. [CrossRef]
21. Wang, Y.; Tu, J.; Li, T.; Tao, C.; Deng, X.; Li, Z. Convenient preparation of $CsSnI_3$ quantum dots, excellent stability, and the highest performance of lead-free inorganic perovskite solar cells so far. *J. Mater. Chem. A* **2019**, *7*, 7683–7690. [CrossRef]
22. Zheng, Y.; Fang, Z.; Shang, M.; Sun, Q.; Zheng, J.; Yang, Z.; Hou, X.; Yang, W. Stabilizing orthorhombic $CsSnI_3$ perovskites with optimized electronic properties by surface ligands with inter-molecular hydrogen bond. *J. Mater. Chem. A* **2021**, *9*, 24641–24649. [CrossRef]
23. Zhang, J.; Yu, C.; Wang, L.; Li, Y.; Ren, Y.; Shum, K. Energy barrier at the N719-dye/$CsSnI_3$ interface for photogenerated holes in dye-sensitized solar cells. *Sci. Rep-UK* **2014**, *4*, 1–6. [CrossRef] [PubMed]
24. Wu, Y.; Chu, W.; Vasenko, A.S.; Prezhdo, O.V. Common Defects Accelerate Charge Carrier Recombination in $CsSnI_3$ without Creating Mid-Gap States. *J. Phys. Chem. Lett.* **2021**, *12*, 8699–8705. [CrossRef]
25. Ma, S.; Gu, X.; Kyaw, A.K.; Wang, D.H.; Priya, S.; Ye, T. Fully Inorganic $CsSnI_3$-Based Solar Cells with >6% Efficiency and Enhanced Stability Enabled by Mixed Electron Transport Layer. *ACS Appl. Mater. Interfaces* **2020**, *13*, 1345–1352. [CrossRef]
26. Chen, Z.; Wang, J.J.; Ren, Y.; Yu, C.; Shum, K. Schottky solar cells based on $CsSnI_3$ thin-films. *Appl. Phys. Lett.* **2012**, *101*, 093901. [CrossRef]
27. Marshall, K.P.; Walker, M.; Walton, R.I.; Hatton, R.A. Enhanced stability and efficiency in hole-transport-layer-free CsSnI3 perovskite photovoltaics. *Nat. Energy* **2016**, *1*, 16178. [CrossRef]
28. Li, B.; Di, H.; Chang, B.; Yin, R.; Fu, L.; Zhang, Y.; Yin, L. Efficient Passivation Strategy on Sn Related Defects for High Performance All-Inorganic $CsSnI_3$ Perovskite Solar Cells. *Adv. Funct. Mater.* **2021**, *31*, 207447. [CrossRef]
29. Ye, T.; Wang, X.; Wang, K.; Ma, S.; Yang, D.; Hou, Y.; Yoon, J.; Wang, K.; Priya, S. Localized Electron Density Engineering for Stabilized B-γ $CsSnI_3$-Based Perovskite Solar Cells with Efficiencies >10%. *ACS Energy Lett.* **2021**, *6*, 1480–1489. [CrossRef]

30. Liu, S.; Tang, Z.-R.; Sun, Y.; Colmenares, J.C.; Xu, Y.-J. One-dimension-based spatially ordered architectures for solar energy conversion. *Chem. Soc. Rev.* **2015**, *44*, 5053–5075. [CrossRef]
31. Xing, G.; Mathews, N.; Sun, S.; Lim, S.S.; Lam, Y.M.; Grätzel, M.; Sum, T.C. Long-range balanced electron-and hole-transport lengths in organic-inorganic $CH_3NH_3PbI_3$. *Science* **2013**, *342*, 344–347. [CrossRef] [PubMed]
32. Eperon, G.E.; Burlakov, V.M.; Docampo, P.; Goriely, A.; Snaith, H.J. Morphological control for high performance, solution-processed planar heterojunction perovskite solar cells. *Adv. Funct. Mater.* **2014**, *24*, 151–157. [CrossRef]
33. Chen, L.-C.; Chen, C.-C.; Chen, J.-C.; Wu, C.-G. Annealing effects on high-performance $CH_3NH_3PbI_3$ perovskite solar cells prepared by solution-process. *Sol. Energy* **2015**, *122*, 1047–1051. [CrossRef]
34. Dualeh, A.; Tétreault, N.; Moehl, T.; Gao, P.; Nazeeruddin, M.K.; Grätzel, M. Effect of annealing temperature on film morphology of organic–inorganic hybrid pervoskite solid-state solar cells. *Adv. Funct. Mater.* **2014**, *24*, 3250–3258. [CrossRef]
35. Zhao, Y.; Zhu, K. Organic–inorganic hybrid lead halide perovskites for optoelectronic and electronic applications. *Chem. Soc. Rev.* **2015**, *45*, 655–689. [CrossRef] [PubMed]
36. Zhang, J.; Hodes, G.; Jin, Z.; Liu, S. All-inorganic CsPbX3 perovskite solar cells: Progress and prospects. *Angew. Chem. Int. Ed.* **2019**, *58*, 15596–15618. [CrossRef]
37. Kim, H.-S.; Im, S.H.; Park, N.-G. Organolead Halide Perovskite: New Horizons in Solar Cell Research. *J. Phys. Chem. C* **2014**, *118*, 5615–5625. [CrossRef]
38. Kieslich, G.; Sun, S.; Cheetham, A.K. Solid-state principles applied to organic–inorganic perovskites: New tricks for an old dog. *Chem. Sci.* **2014**, *5*, 4712–4715. [CrossRef]
39. Rajagopal, A.; Stoddard, R.J.; Hillhouse, H.W.; Jen, A.K.-Y. On understanding bandgap bowing and optoelectronic quality in Pb–Sn alloy hybrid perovskites. *J. Mater. Chem. A* **2019**, *7*, 16285–16293. [CrossRef]
40. Wu, T.; Cui, D.; Liu, X.; Luo, X.; Su, H.; Segawa, H.; Zhang, Y.; Wang, Y.; Han, L. Additive Engineering toward High-Performance Tin Perovskite Solar Cells. *Sol. RRL* **2021**, *5*, 2100034. [CrossRef]
41. Hong, W.-L.; Huang, Y.-C.; Chang, C.-Y.; Zhang, Z.-C.; Tsai, H.-R.; Chang, N.-Y.; Chao, Y.-C. Efficient Low-Temperature Solution-Processed Lead-Free Perovskite Infrared Light-Emitting Diodes. *Adv. Mater.* **2016**, *28*, 8029–8036. [CrossRef] [PubMed]
42. Dimesso, L.; Das, C.; Stöhr, M.; Mayer, T.; Jaegermann, W. Properties of cesium tin iodide (Cs-Sn-I) systems after annealing under different atmospheres. *Mater. Chem. Phys.* **2017**, *197*, 27–35. [CrossRef]
43. Chung, I.; Song, J.H.; Im, J.; Androulakis, J.; Malliakas, C.D.; Li, H.; Freeman, A.J.; Kenney, J.Y.; Kanatzidis, M.G. $CsSnI_3$: Semiconductor or metal? High electrical conductivity and strong near-infrared photoluminescence from a single material. High hole mobility and phase-transitions. *J. Am. Chem. Soc.* **2012**, *134*, 8579–8587. [CrossRef]
44. Liu, S.; Wang, L.; Lin, W.-C.; Sucharitakul, S.; Burda, C.; Gao, X.P.A. Imaging the Long Transport Lengths of Photo-generated Carriers in Oriented Perovskite Films. *Nano Lett.* **2016**, *16*, 7925–7929. [CrossRef] [PubMed]
45. Yang, Y.; Yang, M.; Moore, D.T.; Yan, Y.; Miller, E.M.; Zhu, K.; Beard, M.C. Top and bottom surfaces limit carrier lifetime in lead iodide perovskite films. *Nat. Energy* **2017**, *2*, 16207. [CrossRef]
46. Zeng, W.; Liu, X.; Guo, X.; Niu, Q.; Yi, J.; Xia, R.; Min, Y. Morphology Analysis and Optimization: Crucial Factor Determining the Performance of Perovskite Solar Cells. *Molecules* **2017**, *22*, 520. [CrossRef]
47. Liang, P.-W.; Liao, C.-Y.; Chueh, C.-C.; Zuo, F.; Williams, S.T.; Xin, X.-K.; Lin, J.-J.; Jen, A.K.-Y. Additive Enhanced Crystallization of Solution-Processed Perovskite for Highly Efficient Planar-Heterojunction Solar Cells. *Adv. Mater.* **2014**, *26*, 3748–3754. [CrossRef]
48. Lei, Y.; Li, Y.; Jin, Z. Photon energy loss and management in perovskite solar cells. *Energy Rev.* **2022**, *1*, 100003. [CrossRef]
49. Wang, T.; Yan, F. Reducing Agents for Improving the Stability of Sn-based Perovskite Solar Cells. *Chem.-Asian J.* **2020**, *15*, 1524–1535. [CrossRef]
50. Gu, F.; Zhao, Z.; Wang, C.; Rao, H.; Zhao, B.; Liu, Z.; Bian, Z.; Huang, C. Lead-free tin-based perovskite solar cells: Strategies toward high performance. *Sol. RRL* **2019**, *3*, 1900213. [CrossRef]
51. Calado, P.; Burkitt, D.; Yao, J.; Troughton, J.; Watson, T.M.; Carnie, M.J.; Telford, A.M.; O'Regan, B.C.; Nelson, J.; Barnes, P.R. Identifying Dominant Recombination Mechanisms in Perovskite Solar Cells by Measuring the Transient Ideality Factor. *Phys. Rev. Appl.* **2019**, *11*, 044005. [CrossRef]
52. Wetzelaer, G.-J.A.H.; Scheepers, M.; Sempere, A.M.; Momblona, C.; Ávila, J.; Bolink, H.J. Trap-Assisted Non-Radiative Recombination in Organic-Inorganic Perovskite Solar Cells. *Adv. Mater.* **2015**, *27*, 1837–1841. [CrossRef] [PubMed]
53. Ye, Q.; Zhao, Y.; Mu, S.; Ma, F.; Gao, F.; Chu, Z.; Yin, Z.; Gao, P.; Zhang, X.; You, J. Cesium Lead Inorganic Solar Cell with Efficiency beyond 18% via Reduced Charge Recombination. *Adv. Mater.* **2019**, *31*, e1905143. [CrossRef] [PubMed]
54. Tavakoli, M.M.; Yadav, P.; Prochowicz, D.; Sponseller, M.; Osherov, A.; Bulović, V.; Kong, J. Controllable Perovskite Crystallization via Antisolvent Technique Using Chloride Additives for Highly Efficient Planar Perovskite Solar Cells. *Adv. Energy Mater.* **2019**, *9*, 1803587. [CrossRef]
55. Li, Y.; Wu, H.; Qi, W.; Zhou, X.; Li, J.; Cheng, J.; Zhao, Y.; Li, Y.; Zhang, X. Passivation of defects in perovskite solar cell: From a chemistry point of view. *Nano Energy* **2020**, *77*, 105237. [CrossRef]
56. Marshall, K.P.; Walton, R.I.; Hatton, R.A. Tin perovskite/fullerene planar layer photovoltaics: Improving the efficiency and stability of lead-free devices. *J. Mater. Chem. A* **2015**, *3*, 11631–11640. [CrossRef]
57. Song, T.-B.; Yokoyama, T.; Aramaki, S.; Kanatzidis, M.G. Performance Enhancement of Lead-Free Tin-Based Perovskite Solar Cells with Reducing Atmosphere-Assisted Dispersible Additive. *ACS Energy Lett.* **2017**, *2*, 897–903. [CrossRef]

58. Heo, J.H.; Kim, J.; Kim, H.; Moon, S.H.; Im, S.H.; Hong, K.-H. Roles of SnX_2 (X = F, Cl, Br) Additives in Tin-Based Halide Perovskites toward Highly Efficient and Stable Lead-Free Perovskite Solar Cells. *J. Phys. Chem. Lett.* **2018**, *9*, 6024–6031. [CrossRef]
59. Pitaro, M.; Tekelenburg, E.K.; Shao, S.; Loi, M.A. Tin Halide Perovskites: From Fundamental Properties to Solar Cells. *Adv. Mater.* **2021**, *34*, 2105844. [CrossRef]
60. Kumar, M.H.; Dharani, S.; Leong, W.L.; Boix, P.P.; Prabhakar, R.R.; Baikie, T.; Shi, C.; Ding, H.; Ramesh, R.; Asta, M.; et al. Lead-Free Halide Perovskite Solar Cells with High Photocurrents Realized Through Vacancy Modulation. *Adv. Mater.* **2014**, *26*, 7122–7127. [CrossRef]
61. Mahmoudi, T.; Rho, W.Y.; Kohan, M.; Im, Y.H.; Mathur, S.; Hahn, Y.B. Suppression of Sn^{2+}/Sn^{4+} oxidation in tin-based perovskite solar cells with graphene-tin quantum dots composites in active layer. *Nano Energy* **2021**, *90*, 106495. [CrossRef]
62. Xiang, W.; Tress, W. Review on Recent Progress of All-Inorganic Metal Halide Perovskites and Solar Cells. *Adv. Mater.* **2019**, *31*, e1902851. [CrossRef] [PubMed]
63. Ban, H.; Zhang, T.; Gong, X.; Sun, Q.; Zhang, X.-L.; Pootrakulchote, N.; Shen, Y.; Wang, M. Fully Inorganic $CsSnI_3$ Mesoporous Perovskite Solar Cells with High Efficiency and Stability via Coadditive Engineering. *Sol. RRL* **2021**, *5*, 2100069. [CrossRef]
64. Zhang, T.; Li, H.; Ban, H.; Sun, Q.; Shen, Y.; Wang, M. Efficient $CsSnI_3$-based inorganic perovskite solar cells based on a mesoscopic metal oxide framework *via* incorporating a donor element. *J. Mater. Chem. A* **2020**, *8*, 4118–4124. [CrossRef]
65. Ye, T.; Wang, K.; Hou, Y.; Yang, D.; Smith, N.; Magill, B.; Priya, S.; Mudiyanselage, R.R.H.H.; Khodaparast, G.A.; Wang, K.; et al. Ambient-air-stable lead-free CsSnI3 solar cells with greater than 7.5%. *J. Am. Chem. Soc.* **2021**, *143*, 4319–4328. [CrossRef]
66. Song, T.-B.; Yokoyama, T.; Logsdon, J.L.; Wasielewski, M.R.; Aramaki, S.; Kanatzidis, M.G. Piperazine Suppresses Self-Doping in $CsSnI_3$ Perovskite Solar Cells. *ACS Appl. Energy Mater.* **2018**, *1*, 4221–4226. [CrossRef]
67. Cao, F.; Tian, W.; Wang, M.; Wang, M.; Li, L. Stability enhancement of lead-free $CsSnI_3$ perovskite photodetector with reductive ascorbic acid additive. *Infomat* **2020**, *2*, 577–584. [CrossRef]
68. Song, T.-B.; Yokoyama, T.; Stoumpos, C.C.; Logsdon, J.; Cao, D.H.; Wasielewski, M.R.; Aramaki, S.; Kanatzidis, M.G. Importance of Reducing Vapor Atmosphere in the Fabrication of Tin-Based Perovskite Solar Cells. *J. Am. Chem. Soc.* **2017**, *139*, 836–842. [CrossRef]
69. Tan, S.; Yavuz, I.; De Marco, N.; Huang, T.; Lee, S.; Choi, C.S.; Wang, M.; Nuryyeva, S.; Wang, R.; Zhao, Y.; et al. Steric Impediment of Ion Migration Contributes to Improved Operational Stability of Perovskite Solar Cells. *Adv. Mater.* **2020**, *32*, 1906995. [CrossRef]
70. Chen, J.; Kim, S.G.; Park, N.G. $FA_{0.88}Cs_{0.12}PbI_{3-x}(PF_6)_x$ interlayer formed by ion exchange reaction between perovskite and hole transporting layer for improving photovoltaic performance and stability. *Adv. Mater.* **2018**, *30*, 1801948. [CrossRef]
71. Li, X.; He, B.; Gong, Z.; Zhu, J.; Zhang, W.; Chen, H.; Duan, Y.; Tang, Q. Compositional Engineering of Chloride Ion-Doped $CsPbBr_3$ Halides for Highly Efficient and Stable All-Inorganic Perovskite Solar Cells. *Sol. RRL* **2020**, *4*, 2000362. [CrossRef]
72. Li, C.; Wang, A.; Xie, L.; Deng, X.; Liao, K.; Yang, J.A.; Li, T.; Hao, F. Emerging alkali metal ion (Li^+, Na^+, K^+ and Rb^+) doped perovskite films for efficient solar cells: Recent advances and prospects. *J. Mater. Chem. A* **2019**, *7*, 24150–24163. [CrossRef]
73. Swarnkar, A.; Mir, W.J.; Nag, A. Can B-site doping or alloying improve thermal-and phase-stability of all-inorganic $CsPbX_3$ (X= Cl, Br, I) perovskites? *ACS Energy Lett.* **2018**, *3*, 286–289. [CrossRef]
74. Miyasaka, T.; Kulkarni, A.; Kim, G.M.; Öz, S.; Jena, A.K. Perovskite solar cells: Can we go organic-free, lead-free, and dopant-free? *Adv. Energy Mater.* **2020**, *10*, 1902500. [CrossRef]
75. Marshall, K.P.; Tao, S.; Walker, M.; Cook, D.S.; Lloyd-Hughes, J.; Varagnolo, S.; Wijesekara, A.; Walker, D.; Walton, R.I.; Hatton, R.A. $Cs_{1-x}Rb_xSnI_3$ light harvesting semiconductors for perovskite photovoltaics. *Mater. Chem. Front.* **2018**, *2*, 1515–1522. [CrossRef]
76. Liu, M.; Pasanen, H.; Ali-Löytty, H.; Hiltunen, A.; Lahtonen, K.; Qudsia, S.; Smått, J.-H.; Valden, M.; Tkachenko, N.V.; Vivo, P.; et al. B-Site Co-Alloying with Germanium Improves the Efficiency and Stability of All-Inorganic Tin-Based Perovskite Nanocrystal Solar Cells. *Angew. Chem. Int. Ed.* **2020**, *59*, 22117–22125. [CrossRef] [PubMed]
77. Chen, M.; Ju, M.-G.; Garces, H.F.; Carl, A.D.; Ono, L.K.; Hawash, Z.; Zhang, Y.; Shen, T.; Qi, Y.; Grimm, R.L.; et al. Highly stable and efficient all-inorganic lead-free perovskite solar cells with native-oxide passivation. *Nat. Commun.* **2019**, *10*, 16. [CrossRef] [PubMed]
78. Tang, M.; He, B.; Dou, D.; Liu, Y.; Duan, J.; Zhao, Y.; Chen, H.; Tang, Q. Toward efficient and air-stable carbon-based all-inorganic perovskite solar cells through substituting CsPbBr3 films with transition metal ions. *Chem. Eng. J.* **2019**, *375*, 121930. [CrossRef]
79. Karunakaran, S.K.; Arumugam, G.M.; Yang, W.; Ge, S.; Khan, S.N.; Mai, Y.; Lin, X.; Yang, G. Europium (II)-Doped All-Inorganic CsPbBr3 Perovskite Solar Cells with Carbon Electrodes. *Sol. RRL* **2020**, *4*, 2000390. [CrossRef]
80. Yu, Z.; Hagfeldt, A.; Sun, L. The application of transition metal complexes in hole-transporting layers for perovskite solar cells: Recent progress and future perspectives. *Coord. Chem. Rev.* **2019**, *406*, 213143. [CrossRef]
81. Lee, M.; Yoo, B.; Im, J.; Hyeon, T.; Chung, I. Electronic band engineering via MI_3 (M= Sb, Bi) doping remarkably enhances the air stability of perovskite $CsSnI_3$. *ACS Appl. Energy Mater.* **2020**, *3*, 10477–10484. [CrossRef]
82. Jeong, J.; Kim, M.; Seo, J.; Lu, H.; Ahlawat, P.; Mishra, A.; Yang, Y.; Hope, M.A.; Eickemeyer, F.T.; Kim, M.; et al. Pseudo-halide anion engineering for α-$FAPbI_3$ perovskite solar cells. *Nature* **2021**, *592*, 381–385. [CrossRef] [PubMed]
83. Xu, Z.; Chen, R.; Wu, Y.; He, R.; Yin, J.; Lin, W.; Wu, B.; Li, J.; Zheng, N. Br-containing alkyl ammonium salt-enabled scalable fabrication of high-quality perovskite films for efficient and stable perovskite modules. *J. Mater. Chem. A* **2019**, *7*, 26849–26857. [CrossRef]

84. Yusoff, A.R.B.M.; Vasilopoulou, M.; Georgiadou, D.G.; Palilis, L.C.; Abate, A.; Nazeeruddin, M.K. Passivation and process engineering approaches of halide perovskite films for high efficiency and stability perovskite solar cells. *Energy Environ. Sci.* **2021**, *14*, 2906–2953. [CrossRef]
85. Zhang, X.; Zhou, W.; Chen, X.; Chen, Y.; Li, X.; Wang, M.; Zhou, Y.; Yan, H.; Zheng, Z.; Zhang, Y. Dual Optimization of Bulk and Surface via Guanidine Halide for Efficient and Stable 2D/3D Hybrid Perovskite Solar Cells. *Adv. Energy Mater.* **2022**, *12*, 2201105. [CrossRef]
86. Sabba, D.; Mulmudi, H.K.; Prabhakar, R.R.; Krishnamoorthy, T.; Baikie, T.; Boix, P.P.; Mhaisalkar, S.; Mathews, N. Impact of Anionic Br^- Substitution on Open Circuit Voltage in Lead Free Perovskite ($CsSnI_{3-x}Br_x$) Solar Cells. *J. Phys. Chem. C.* **2015**, *119*, 1763–1767. [CrossRef]
87. Zhao, Z.; Wu, J.; Fang, F.; Li, T.; Zhou, Y.; Wang, J. The mechanism of the stability improvement of the Bγ-$CsSnI_3$ perovskite doped with fluorine. *Mater. Res. Express* **2019**, *6*, 125534. [CrossRef]
88. Zhu, P.; Chen, C.; Gu, S.; Lin, R.; Zhu, J. $CsSnI_3$ Solar Cells via an Evaporation-Assisted Solution Method. *Sol. RRL* **2018**, *2*, 1700224. [CrossRef]
89. Li, J.; Huang, J.; Zhao, A.; Li, Y.; Wei, M. An inorganic stable Sn-based perovskite film with regulated nucleation for solar cell application. *J. Mater. Chem. C* **2020**, *8*, 8840–8845. [CrossRef]
90. Kiyek, V.M.; Birkhölzer, Y.A.; Smirnov, Y.; Ledinsky, M.; Remes, Z.; Momand, J.; Kooi, B.J.; Koster, G.; Rijnders, G.; Morales-Masis, M. Single-source, solvent-free, room temperature deposition of black γ-$CsSnI_3$ films. *Adv. Mater. Interfaces* **2020**, *7*, 2000162. [CrossRef]
91. Chen, H. Two-Step Sequential Deposition of Organometal Halide Perovskite for Photovoltaic Application. *Adv. Funct. Mater.* **2017**, *27*, 1605654. [CrossRef]
92. Zhao, P.; Kim, B.J.; Ren, X.; Lee, D.G.; Bang, G.J.; Jeon, J.B.; Bin Kim, W.; Jung, H.S. Antisolvent with an Ultrawide Processing Window for the One-Step Fabrication of Efficient and Large-Area Perovskite Solar Cells. *Adv. Mater.* **2018**, *30*, e1802763. [CrossRef]
93. Liu, J.; Li, N.; Jia, J.; Dong, J.; Qiu, Z.; Iqbal, S.; Cao, B. Perovskite films grown with green mixed anti-solvent for highly efficient solar cells with enhanced stability. *Sol. Energy* **2019**, *181*, 285–292. [CrossRef]
94. Wang, N.; Zhou, Y.; Ju, M.G.; Garces, H.F.; Ding, T.; Pang, S.; Zeng, X.; Padture, N.P.; Sun, X.W. Heterojunction-depleted lead-free perovskite solar cells with coarse-grained B-γ-$CsSnI_3$ thin films. *Adv. Energy Mater.* **2016**, *6*, 1601130. [CrossRef]
95. Ban, H.; Nakajima, T.; Liu, Z.; Yu, H.; Sun, Q.; Dai, L.; Shen, Y.; Zhang, X.-L.; Zhu, J.; Chen, P.; et al. Over 8% efficient $CsSnI_3$-based mesoporous perovskite solar cells enabled by two-step thermal annealing and surface cationic coordination dual treatment. *J. Mater. Chem. A* **2022**, *10*, 3642–3649. [CrossRef]

Disclaimer/Publisher's Note: The statements, opinions and data contained in all publications are solely those of the individual author(s) and contributor(s) and not of MDPI and/or the editor(s). MDPI and/or the editor(s) disclaim responsibility for any injury to people or property resulting from any ideas, methods, instructions or products referred to in the content.